5B.4 INVESTIGATING CONVECTIVE SCALE VARIABILITY IN TROPICAL CYCLONE RAINBAND CLOUDS AND DYNAMICS USING COMPACT RAMAN LIDAR MEASUREMENTS

Ethan J. Murray[1,2], Jason P. Dunion[3], Kristopher B. Karnauskas[1, 4], Zhien Wang[5], and Jun A. Zhang[3, 6]

[1] Department of Atmospheric and Oceanic Sciences, University of Colorado, Boulder, CO
[2] Laboratory for Atmospheric and Space Physics, University of Colorado, Boulder, CO
[3] NOAA/AOML Hurricane Research Division, Miami, FL
[4] Cooperative Institute for Research in Environmental Sciences, University of Colorado, Boulder, CO
[5] School of Marine and Atmospheric Sciences, Stony Brook University, Stony Brook, NY
[6] Cooperative Institute for Marine and Atmospheric Studies, University of Miami, Miami, FL

1. INTRODUCTION

Due to their elevated precipitation rates and strong winds, tropical cyclone (TC) rainbands cause significant coastal damage during landfall events. Both internal and environmental factors control rainband formation. Dry air entrainment from the nearby environment and strong environmental wind shear suppress rainband development (Alland et al. 2021; Barnes et al. 1983, p. 198), while individual rainbands can weaken TC winds by cutting off the inward advection of θ_e to the eyewall (Powell 1990).

Different TCs often share similar rainband structures. These similarities are a function of their position within the TC relative to the environmental shear vector. This vector creates four shear relative quadrants: the downshear right (DR), downshear left (DL), upshear left (UL), and upshear right (UR) quadrants. A principal rainband, also known as a stationary band complex, often forms downshear and experiences the deepest convection and strongest precipitation (Didlake and Houze 2013a; Hence and Houze Jr. 2008). Stratiform sectors ring the principal rainband, and the least convection is found in the UR quadrant (Barron et al. 2022; Didlake and Houze 2013b). These cloud formations are tied to boundary layer thermodynamics, with boundary layer recovery aiding convective growth downshear and dry subsidence hindering it upshear (Zhang et al. 2013).

The relationships between low level rainband clouds, thermodynamics, and dynamics remain poorly constrained. While radar measurements display the location of heavy precipitation, low level rainband cloud tops have not been observed. Here, we use novel lidar-based aircraft observations combined with existing radar and in situ measurements to fill in measurement gaps and view TC rainband structure with unprecedented detail. These methods link typical rainband features to TC internal structures and environmental conditions as well as their underlying physical processes. Case studies and statistics are used to address these knowledge gaps.

* *Corresponding author address:* Ethan Murray, University of Colorado, Boulder, Department of Atmospheric and Oceanic Sciences, 4001 Discovery Drive, Boulder, CO, 80303. Email: ethan.murray@colorado.edu

2. OBSERVATIONAL DATASETS AND METHODS

The novel compact Raman lidar (CRL) measures atmospheric temperature, water vapor, and backscattered power below the P-3 aircraft. CRL data were collected from nine TCs in 2021 and 2022. These data are confined to the lowest 3 km of the troposphere, and their 6 m vertical and 250 m horizontal resolution provides detailed thermodynamic and microphysical information. Backscattered power channel returns distinguish between cloud tops, entrained rainfall, surface layer aerosols, and clear air.

CRL measurements are collocated with tail Doppler radar (TDR) and in situ data to view TC rainbands. Flight level winds are used to calculate the radius of maximum wind (RMW) for each TC, which is then used to normalize distances in the composite plot below (Figure 4). TDR reflectivity and wind fields provide useful views of TC dynamics and precipitation, and they complement the CRL profiles. Level 3 swath TDR data (2500 m horizontal, 500 m vertical resolution) are used for the 3D precipitation partitions in Figure 2, while Level 2 profile data (1500 m horizontal, 150 m vertical resolution) are used for the along leg calculations in Figures 1 and 4.

Two new algorithms were recently developed to automate the detection of CRL-based rainfall regions and cloud tops. The cloud top identification code finds tops based on strong return power peaks, while the rainfall algorithm looks for elevated power signals without sharp peaks that originate near flight height and extend towards the surface. Both these algorithms accurately depict cloud and rainfall regions for all cases in the CRL database.

An example P-3 pass through TC Sam on 9/26/21 is shown below (Figure 1b). Both low level rainfall and cloud returns are encountered in the UL quadrant, while Sam's DR rainband contains scattered rainfall regions and many tall cloud tops. The cloud top and rainfall algorithms discussed above correctly identify these features, allowing for subsequent statistical tests using all CRL power profiles.

3. CASE STUDY: TC SAM

On September 26th, 2021, Sam was a strong, Category 4 Atlantic TC east of the Lesser Antilles. At its time of sampling, Sam had an interpolated intensity of 67.5 m/s (936.75 hPa) and was about to experience a rapid weakening event due to an eyewall replacement cycle. Sam was also impacted by moderate, southwesterly vertical wind shear with a strength of 4.5 m/s. This is an ideal case study for viewing the TC rainbands because of the abundant CRL and TDR data, Sam's strong intensity, and its shear impacted structure.

3D TDR swath measurements confirm the asymmetric nature of TC Sam's reflectivity and precipitation structure. Based upon the orientation of the shear vector, reflectivity at 2 km height on Sam's left side is upshear, while reflectivity to its right is downshear (Figure 2a). Focusing on the rainbands, high reflectivity reaches from the eyewall out through the head of the principal rainband in the UL quadrant, matching previous conceptual models depicting this structure (Barron et al. 2022). The DR quadrant is more complex, as a gap of lower reflectivity separates two high reflectivity regions. This could be due to radial ventilation of Sam's rainband with the dry Saharan Air Layer at midlevels (Alland et al. 2021).

The 3D swath TDR reflectivity field is used by an empirical algorithm to observationally derive Sam's precipitation types. This algorithm has been implemented successfully in previous studies (Wadler et al. 2023). Sam's upshear principal rainband was classified as moderate convective cells bounded by stratiform regions (Figure 2b). Sam's downshear regions only have moderate convection outside the eyewall and in the distant rainbands; the rest of the area is filled with stratiform clouds and weak echoes.

The profile view of Sam's TDR reflectivity structure further highlights the shear induced asymmetry found in this TC (Figure 1a). Sam's UL rainband has strong reflectivity retrievals extending from the left eyewall out to -100 km. Once again, a convective gap separates two high reflectivity regions in Sam's DR quadrant. Evidence of a melting layer appears around 5 km height in the profile view, especially in the UL quadrant, suggesting more stratiform rain than previously expected.

Despite strong UL TDR reflectivity, the CRL power channel reveals that low level clouds only extend out to 70 km, not to the 100 km seen previously. The outer 30 km of this rainband is composed of rainfall advected from above, with cloud free air nearly reaching the surface. This suggests that the outer portion of Sam's UL rainband is stratiform in nature, rather than convective. The existence of the stratiform moat between the UL eyewall and inner rainband seen around x=-20 km is confirmed by the CRL dataset (Figure 2b). This moat of weak rainfall and low clouds could be from suppressed convection due to poor boundary layer recovery (Powell 1990).

In the DR quadrant, the CRL resolves the two convective cloud bands seen by the TDR flanking the eyewall and those forming outside 125 km from the TC center (Figure 1b). Additionally, the CRL displays unique cloud features missed by the TDR. While the TDR only shows a few isolated, low level clouds in the convective gap, the CRL shows this region is filled with low level convective cells(examples are centered around 70 km and 105 km). The existence of these features is confirmed by the empirical rainfall and cloud top algorithms (Figure 1c), suggesting that radial ventilation isn't heavily impacting low level convection in Sam's DR quadrant.

Overall, CRL power measurements better elucidate the role of low level clouds in the evolution of TC Sam's rainbands. Based solely on TDR observations, it appears that the UL quadrant contains moderate convection from the left eyewall to -100 km. But, using the CRL's power channel, the outer portion of this rainband is revealed to be stratiform rainfall advected from above. Likewise, using the TDR, the DR quadrant appears to be devoid of significant convection between two prominent rainband features. The CRL, however, highlights that significant low level convection actually builds in this area.

This analysis of CRL measurements better matches conceptual models of shear induced rainband cloud formation, reinforcing our understanding. For example, low level convection begins to build in the DR quadrant, which is confirmed by CRL data in this case. Similarly, the UL quadrant sees extensive but eroding convection, once again best matching low level CRL observations (Barron et al. 2022).

4. STATISTICAL ANALYSIS

Using all available aircraft measurements from 2021 and 2022, CRL and TDR statistics illuminate differences between rainband shear quadrants. Building upon previous studies, low level cloud tops and rainfall regions are calculated using the same algorithms outlined in Figure 1. This process was repeated for all 61 radial legs with CRL and TDR data. By focusing on actual cloud top measurements in the lowest 3 km of the atmosphere, this study clarifies the role of low level clouds in asymmetric convective development and extends our understanding of shear quadrant differences to the TC boundary layer and the region just above it.

The first cloud fraction test uses a height limit of 1500 m, since this region is often at the height of the inflow boundary layer (Zhang et al. 2013). Boundary layer cloud top fractions are highest downshear, with mean values of

0.53 and 0.54 in DR and DL regions, respectively (Figure 3a). Upshear quadrants are more cloud free with mean values of 0.42 and 0.41 in UL and UR regions, respectively. That downshear quadrants have over 10% more boundary layer clouds than upshear quadrants suggests that low level clouds build downshear and dissipate upshear, consistent with the canonical understanding of TC rainband cloud development.

Since boundary layer cloud bases are typically below 2700 m in height in TC rainbands, and that this is close to P-3 flight height, cloud fractions are calculated at this level to diagnose convective cloud distributions (Figure 3b). The DL quadrant has the highest mean convective cloud fraction at 0.26, while the UR quadrant is lowest at 0.10. Convective proportions are similar for DR and UL quadrants with values of 0.19 and 0.17. These findings show that low level convection builds DR, peaks DL, erodes UL, and is dissipated UR, in agreement with previous observations focused on deep convection (Wadler et al. 2023).

Rainfall fractions highlight another TC shear quadrant asymmetry (Figure 3c). Rainfall is most prevalent UL, covering a mean of 38% of scenes, and it is least prevalent UR, comprising only 28% of rainfall pixels. This reinforces our understanding of the TC rainbands, with precipitation increasing in association with the principal rainband in DR and DL quadrants, and with the most rainfall found UL due to heightened precipitation from collapsing convection (Wadler et al. 2023).

Secondary circulation patterns derived from TDR wind observations explain CRL cloud fraction results (Figure 4). The DR quadrant has the deepest inflow layer (negative radial wind) and most extensive upward motion in the rainbands of any quadrant. As seen previously, this region is where convection initiates, as frequent boundary layer clouds form here. Winds in the DL quadrant also complement observed cloud and rainfall distributions, as this region has a tall, well defined inflow layer and some upward vertical motion, matching the tall convective clouds and moderate rainfall distributions seen previously (Barron et al. 2022).

Upshear quadrants have the opposite wind distributions. The UL and especially the UR quadrant have limited inflow layers, often not even reaching 500 m (Zhang et al. 2013). Besides some distant upward motion beyond r*=4 in the DR quadrant, both cases experience extensive rainband subsidence. Upshear quadrant dynamics contribute to the limited upshear rainband cloud formation and convection. This shift towards more UL downdrafts also explains enhanced UL rainfall seen in Figure 3c; this rain is likely advected downwards by decaying convection into the quadrant's clear air regions.

5. DISCUSSION

A novel CRL observational dataset builds upon previous techniques and illuminates the shear dependence of TC rainband clouds. A case study of TC Sam distinguishes rainband cloud and rainfall features from UL and DR quadrants. When viewing these structures using CRL return power profiles, more precipitation is found in the UL quadrant, and enhanced low level clouds are seen DR. These findings display the heightened complexity of low level rainband structures seen when using CRL backscattered power returns, filling measurement gaps in previous techniques.

This analysis is extended to all TC cases, finding that low level, boundary layer cloud fractions peak downshear, with low level convective clouds mostly found DL. Furthermore, rainfall fractions peak UL, as this region is associated with collapsing convection near the head of the principal rainband. Differences in radial and vertical velocity partitions support the existence of these rainband asymmetries.

This research reminds us that TC rainbands are highly complex, while reinforcing that they share similar shear-induced asymmetries. These asymmetries are driven by low level thermodynamic differences, cycling based on shear quadrant (Zhang et al. 2013). A promising aspect of the CRL instrument is its ability to obtain temperature and water vapor profiles, which can be used to link the aforementioned cloud and rainfall observations to convective scale thermodynamics.

6. ACKNOWLEDGEMENTS

This research is supported by ONR Grant N00014-21-1-2606 through the TCRI Departmental Research Initiative. The authors also thank the scientists and employees of NOAA / AOML / HRD who facilitated the deployment and operation of the CRL.

7. REFERENCES

Alland, J. J., B. H. Tang, K. L. Corbosiero, and G. H. Bryan, 2021: Combined Effects of Midlevel Dry Air and Vertical Wind Shear on Tropical Cyclone Development. Part II: Radial Ventilation. *Journal of the Atmospheric Sciences*, **78**, 783–796, https://doi.org/10.1175/JAS-D-20-0055.1.

Barnes, G. M., E. J. Zipser, D. Jorgensen, and F. Marks, 1983: Mesoscale and Convective Structure of a Hurricane Rainband. *Journal of the Atmospheric Sciences*, **40**, 2125–2137, https://doi.org/10.1175/1520-0469(1983)040<2125:MACSOA>2.0.CO;2.

Barron, N. R., A. C. Didlake Jr., and P. D. Reasor, 2022: Statistical Analysis of Convective Updrafts in Tropical Cyclone Rainbands Observed by

Airborne Doppler Radar. *Journal of Geophysical Research: Atmospheres*, **127**, e2021JD035718, https://doi.org/10.1029/2021JD035718.

Didlake, A. C., and R. A. Houze, 2013a: Convective-Scale Variations in the Inner-Core Rainbands of a Tropical Cyclone. *Journal of the Atmospheric Sciences*, **70**, 504–523, https://doi.org/10.1175/JAS-D-12-0134.1.

——, and ——, 2013b: Dynamics of the Stratiform Sector of a Tropical Cyclone Rainband. *Journal of the Atmospheric Sciences*, **70**, 1891–1911, https://doi.org/10.1175/JAS-D-12-0245.1.

Hence, D. A., and R. A. Houze Jr., 2008: Kinematic structure of convective-scale elements in the rainbands of Hurricanes Katrina and Rita (2005). *Journal of Geophysical Research: Atmospheres*, **113**, https://doi.org/10.1029/2007JD009429.

Powell, M. D., 1990: Boundary Layer Structure and Dynamics in Outer Hurricane Rainbands. Part II: Downdraft Modification and Mixed Layer Recovery. *Monthly Weather Review*, **118**, 918–938, https://doi.org/10.1175/1520-0493(1990)118<0918:BLSADI>2.0.CO;2.

Wadler, J. B., J. J. Cione, R. F. Rogers, and M. S. Fischer, 2023: On the Distribution of Convective and Stratiform Precipitation in Tropical Cyclones from Airborne Doppler Radar and Its Relationship to Intensity Change and Environmental Wind Shear Direction. *Monthly Weather Review*, **151**, 3209–3233, https://doi.org/10.1175/MWR-D-23-0048.1.

Zhang, J. A., R. F. Rogers, P. D. Reasor, E. W. Uhlhorn, and F. D. Marks, 2013: Asymmetric Hurricane Boundary Layer Structure from Dropsonde Composites in Relation to the Environmental Vertical Wind Shear. *Monthly Weather Review*, **141**, 3968–3984, https://doi.org/10.1175/MWR-D-12-00335.1.

8. FIGURES

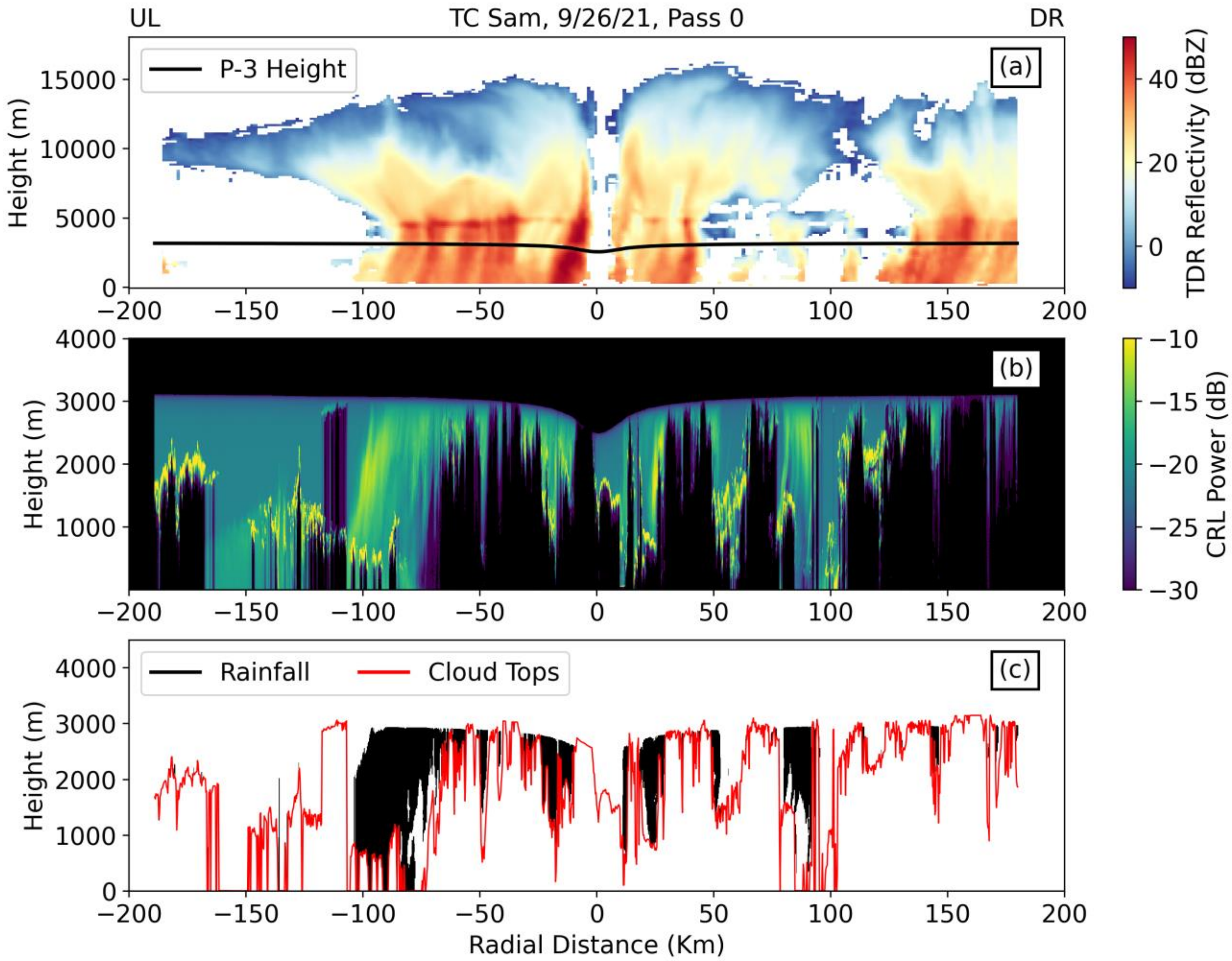

Figure 1: Profile views of TC Sam's radial structure on 9/26/21 using TDR reflectivity (a) and CRL return power (b) channels. Shear quadrants are denoted above (a). Black regions in (b) depict areas of total CRL power attenuation below cloud tops. Regions of high backscatter from cloud tops have values around -10 dB, precipitation and boundary layer aerosols are between -12.5 dB and -17.5 dB, and clear air has return strengths around -20 dB. Panel (c) highlights CRL-determined cloud tops and rainfall regions using two new algorithms discussed in the main text.

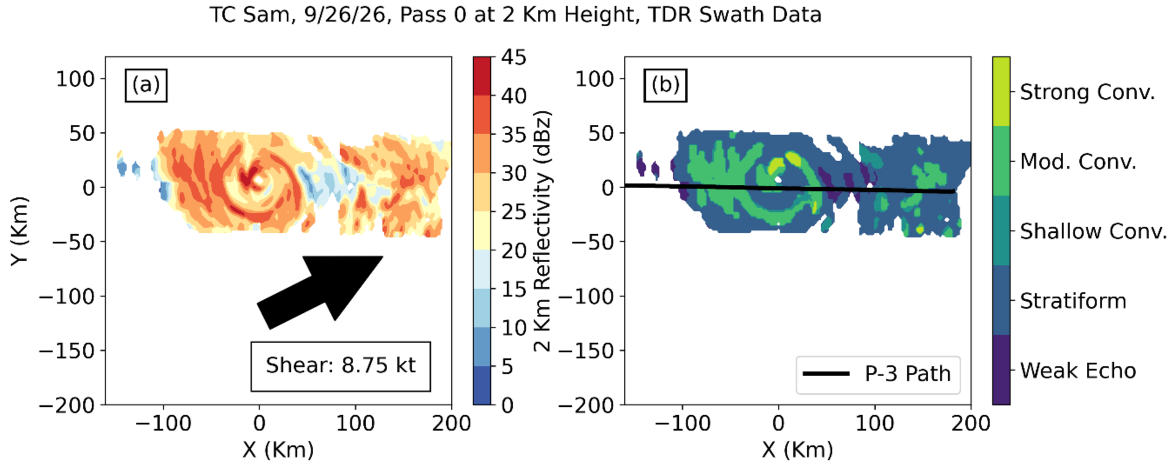

Figure 2: Plan view of TC Sam's 2 km height TDR swath reflectivity field (a) and rainfall type partition (b). The black line in (b) represents the P-3 flight path shown in Figure 2.

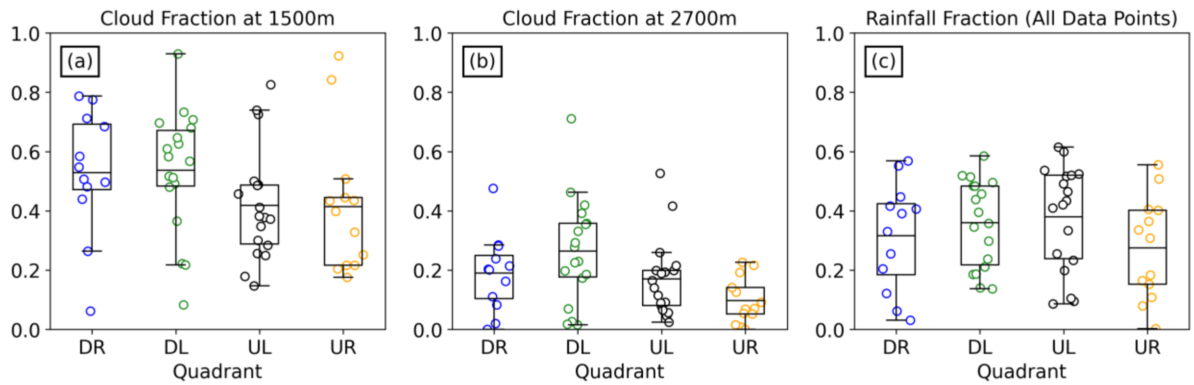

Figure 3: CRL-determined rainband cloud fractions taken at 1500 m (a) and 2700 m (b) heights, along with full column rainband rainfall fractions (c), partitioned by shear quadrant. Box plots range from the first to the third quartile, with the mean represented as a central black line. Whiskers reach from box edges to the furthest data point within 1.5 times the interquartile range. Each scatter point represents cloud or rainfall fractions from one radial leg. Cloud fractions are calculated as the ratio of cloud heights above a given threshold, and rainfall fractions are the proportion of rainfall versus all air regions above cloud tops.

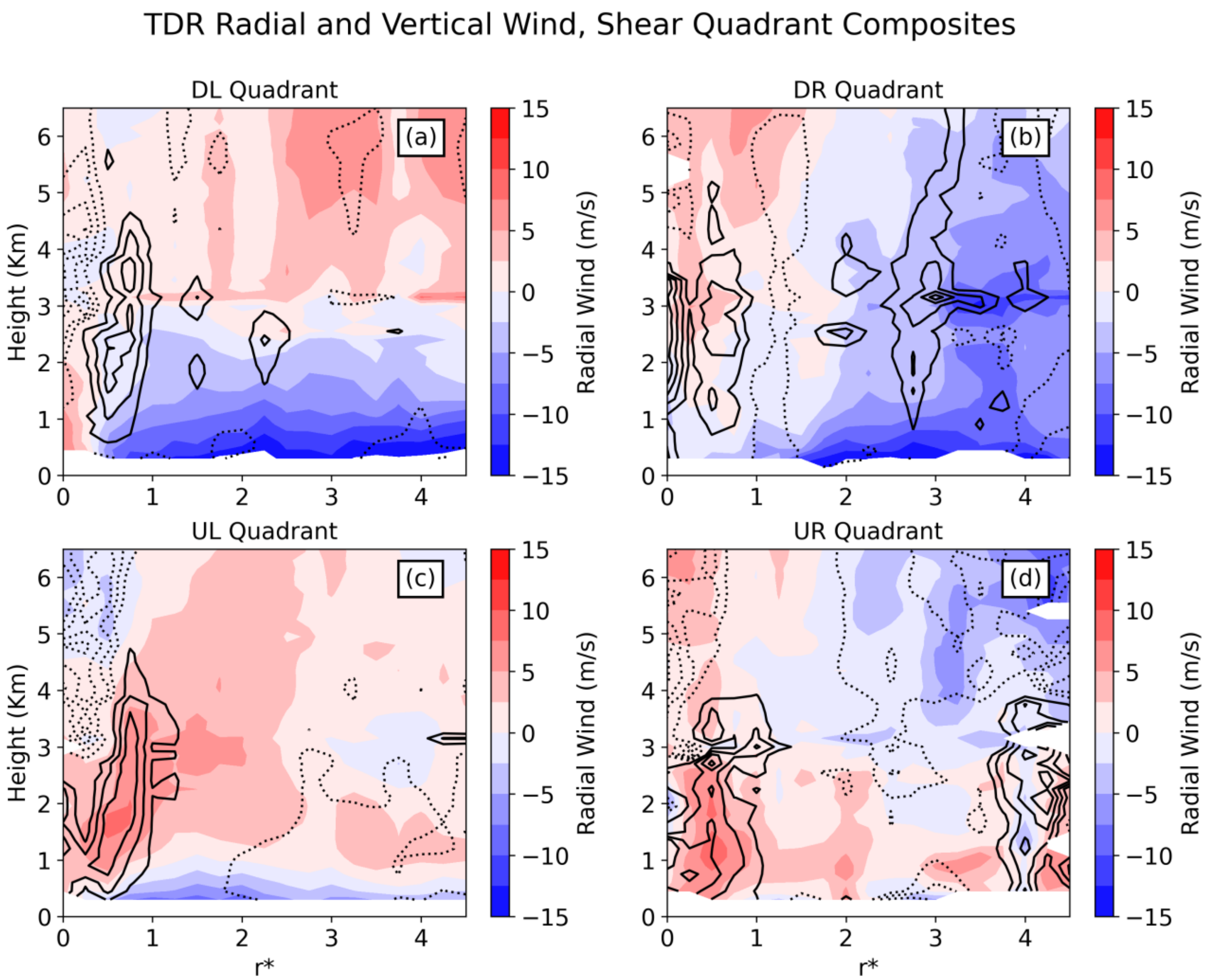

Figure 4: Shear quadrant partitions of TDR radial velocity (shading) and vertical velocity (black contours) from 2021 and 2022 cases with CRL profiles. Solid (dashed) contours represent positive (negative) vertical velocities at 0.5 m/s intervals. The rainbands are located roughly from r*=1.5 to r*=4.